scientific reports

OPEN

Biogenic silver nanoparticles incorporated hydrogel beads for anticancer and antibacterial activities

Vyshnavi T. Veetil[1,2,3], Vidhu Jayakrishnan[1,2,3], Vaisakh Aravindan[1,2], Anakha D. Rajeeve[1,2], Sreekanth Koolath[1,2] & Ramasamy Yamuna[1,2]✉

Green nanotechnology is an effective treatment approach being used in cancer research with less adverse effects. This work describes the incorporation of silver nanoparticles synthesized from clitoria ternatea plant extract (Ag@*CT* NPs) into sodium alginate and gelatin polymer blends (SA/GEL) to produce Ag@*CT*-SA/GEL polymer beads using calcium chloride ($CaCl_2$) crosslinking agent. Both the formation and the effective incorporation of Ag@*CT* NPs into polymer blend have been proven by various spectroscopic analysis, surface morphology study and energy dispersive X-ray analysis. Ag@*CT* NPs and Ag@*CT*-SA/GEL demonstrate good antibacterial and antioxidant activities comparable to commercially available drug. Dimethyl thiazolyl tetrazolium bromide (MTT) anticancer assay and apoptosis study of plant extract and Ag@*CT* NPs against lung cancer cell lines clearly indicate that Ag@*CT*-SA/GEL polymer bead can serve as an effective anticancer agent.

Keywords Silver nanoparticle, Sodium alginate, Gelatin, Anticancer, Antioxidant, Antibacterial

Lung cancer is the most diagnosed cancer, accounting 18.4% of the cancer-related fatalities globally[1]. The GLOBOCON research predicts that by 2040, the global incidence rate of lung cancer would rise by 66.7%, while the fatality rate will increase by 59.8%[1]. The high death rate from lung cancer is attributed to the cancer habitat which includes smoking, lack of physical activity, and a contemporary lifestyle. Lung cancer is usually treated with a range of therapeutic techniques, such as chemotherapy, radiation, radiosurgery, and immunotherapy. A suitable treatment for lung cancer is determined by the patient's clinical evaluation, the phase of the illness, and its pathological type. The most effective method of treating lung cancer is surgery. However, this is not appropriate for advanced or metastatic stages of the disease. Especially, chemotherapeutic methods can cause cancer resistance to therapy along with adverse side effects. Therefore, there is a growing need to develop intriguing, affordable, and biocompatible drugs for treating lung cancer. Green nanotechnology would be a promising treatment method for lung cancer.

Nanoparticles (NPs) offer unique features, such as a high surface-to-volume ratio and good absorption profile in the visible region. This makes them ideal for antibacterial, and anticancer applications[2–6]. Silver nanoparticles (Ag NPs) are attracting enormous amount of interest in cancer research due to their unique physicochemical characteristics and innate antiproliferative effect. Silver demonstrates least toxicity that is owing to the human body's competent physiological detoxification system[7]. Several in vitro and in vivo studies have revealed that Ag NPs can trigger apoptosis and necrosis by inducing DNA damage[8–10]. Green synthetic methods of silver nanoparticles are more beneficial than chemical synthesis. This biogenic Ag NPs have a phytochemical covering that makes them more physiologically active. Further, these biogenic NPs can maintain their beneficial anti-cancer cell-toxicity against a range of cancer cell while having less side effects[11–13].

Clitoria ternatea (*CT*), a member of the Fabaceae family and a popular gardening flower in India, is renowned for its therapeutic benefits. It improves memory and is used to treat several diseases including tumor, dropsy, goiter, leprosy, elephantiasis, and chronic bronchitis[14]. *CT* is a rich source for polyphenols such as various flavanol glycosides of kaempferol, quercetin, and myricetin along with ternatin anthocyanins[15]. These flavonoids are known for their wide range of anticancer potential towards various cancer cell[16,17]. The crude extracts from

[1]Department of Chemistry, Amrita School of Physical Sciences, Amrita Vishwa Vidyapeetham, Coimbatore, India. [2]Bio-Materials Chemistry Research Laboratory, Amrita School of Engineering, Amrita Vishwa Vidyapeetham, Coimbatore, India. [3]These authors are contributed equally: Vyshnavi T. Veetil and Vidhu Jayakrishnan. ✉email: r_yamuna@cb.amrita.edu

different sections of *CT* plants show apparent cytotoxic properties against several in vitro human cancer cell lines[18–20]. Literature reports reveal in vitro antioxidant activity of *CT* stem bark extract[21]. The leaves, roots, stems, and pods of *CT* have all been previously described as natural reducing and capping agents for the inorganic NPs[22–24]. *CT* flower extract has been utilized mainly for the synthesis of silver and gold nanoparticles[25]. There are few studies that reported the synthesis of Ag NPs using *CT* plant extract and evaluated their antimicrobial activity[22,23]. Srinivas et al. has shown the synthesis of biogenic Ag NPs using *CT* flower extract and evaluated its anticancer properties against breast cancer[26].

Variations in pH and presence of digestive enzymes like pepsin and pancreatin are the main cause of polyphenols degradation across the gastrointestinal tract (GIT)[27]. To preserve their structural integrity before reaching the gut, oral delivery of these bioactive substances necessitates the development of a new approach that gives protection from gastric and intestinal digestion[28]. Thus, these polyphenols can be encapsulated in biodegradable polymer bead as a strategy to boost bioavailability and overcome biological barriers.

Sodium alginate (SA) is a natural biopolymer derived from brown seaweed with good biocompatibility, swelling, biodegradability, cell viability, drug encapsulation capabilities, gelation, and stabilization properties[29–31]. This dimeric copolymer is unbranched and consists of two types of monomers, namely β-D-mannuronic acid (M) and α-L-glucuronic acid (G), connected by 1,4-glycosidic linkages. These monomers are arranged in blocks of MM, GG, and MG in an alternate manner. SA hydrogel is often employed to transport hydrophilic bioactive substances[32,33]. Gelatin (GEL) is a natural biopolymer derived from collagen, making it biocompatible and well-tolerated by the body. It is susceptible to enzymatic degradation by proteases present in the body[34]. This characteristic enables the controlled release of encapsulated drugs and the gradual degradation of the GEL matrix over time. SA creates an egg-box-shaped three-dimensional network hydrogel by means of electrostatic interaction between the guluronic acid and the interchange of guluronic acid's sodium ions with divalent cations like calcium (Ca^{2+}), magnesium (Mg^{2+}), barium (Ba^{2+}), and strontium (Sr^{2+})[35]. Calcium alginate hydrogels possess several drawbacks, such as uncontrollable swelling and drug release profile due to the natural stiffness of Ca^{2+} alginate[36]. Calcium alginates beads are mixed with GEL, to generate a complex structure through electrostatic interactions and hydrogen bonding interactions. Therefore, these combinations of polymers are suitable for the controlled drug release rate and swelling properties. The combination of GEL's cell-interactive features with SA's gelation capabilities can yield synergistic benefits.

Ag NPs produced using *CT* offers sustainable and non-toxic approach to treat lung cancer and bacterial infection on a single platform. Moreover, this approach is more crucial because lung cancer patients are vulnerable to microorganism[37,38]. The SA/GEL bead system enables controlled release, biocompatibility, and targeted delivery. Therefore, this innovative system can be built in low cost and scalable way for wide range of biological applications.

The current work reports the incorporation of synthesized Ag@*CT* NPs into the SA/GEL polymer blends to form beads through $CaCl_2$ crosslinking process. The formation of Ag@*CT* and its effective incorporation into SA/GEL polymer bead has been studied by various spectroscopic and surface morphological analysis. The anticancer potential of *CT* plant extract and Ag@*CT* NPs towards A549 lung cancer cell line was determined by conducting dimethyl thiazolyl tetrazolium bromide (MTT) and acridine orange/ethidium bromide (AO/EB) staining assays. Further, antibacterial and antioxidant studies of Ag@*CT* NPs and Ag@*CT*-SA/GEL have been reported.

Materials and methods

Materials

For the synthesis of Ag@*CT*-SA/GEL polymer beads, silver nitrate [($AgNO_3$); SRL Chemicals], sodium hydroxide [(NaOH); Fisher Scientific] were used. Calcium chloride [($CaCl_2$); Himedia], sodium alginate [SRL Chemicals] and gelatin [Nice Chemicals] were obtained and used without any additional purification.

Green synthesis of Ag@CT NPs

Ag@*CT* NPs were synthesized using aqueous plant extract of *CT* in accordance with the recently reported procedure from our lab[39]. The stem and leaves of *CT* plant were collected from the Amrita Vishwa Vidyapeetham (Deemed to be University), Coimbatore campus by following the relevant guidelines and regulations set by the University. To ensure the reproducibility of the study, a voucher representing the specimen is identified by Dr. M. U. Sharief and it has been deposited in the herbarium at the Botanical Survey of India, Coimbatore under the accession number 178359. In brief, the stem and leaves of the *CT* were rinsed with double distilled water (DDW) and then they were let to dry for 6 h. After being dehydrated for 6 h, the stem and leaves were ground into a fine powder and placed inside an airtight container. For the extract preparation, a 0.01 g of *CT* powder was dissolved in 20 mL of DDW by ultrasonicating it for 10 min. The extract was then filtered through Whatman No. 41 filter paper and stored at 4 °C. In order to synthesize Ag@*CT* NPs, 20 mL of the *CT* extract was gradually added to 6 mL of 6 mM $AgNO_3$ solution. Then, 0.1 M NaOH solution was added to bring the pH of the mixture to 10, and it was heated at 70 °C on a hot plate. After 15 min, the colorless $AgNO_3$ solution turned to an intense brown suggesting the reduction of Ag^+ to Ag^o. Finally, the green synthesized Ag@*CT* NPs were obtained by centrifugation for 15 min at 15,000 rpm.

Preparation of Ag@CT-SA/GEL polymer bead

Primarily, 2% of SA and 2% of GEL in DDW were made separately by stirring them at 350 rpm for 20 min in room temperature, yielding a homogenous polymer solution. Then, equal volumes of these polymer solutions were mixed together with 2% Ag@*CT* NPs and stirred at 350 rpm for 30 min in room temperature to produce a homogeneous solution. Later, SA/GEL polymer solution containing Ag@*CT* NPs was added dropwise using 0.55 mm syringe into 3% $CaCl_2$ solution under continuous stirring at 300 rpm in room temperature. This reaction mixture was stirred overnight to facilitate crosslinking and the resulting polymer beads were filtered and washed with DDW to eliminate the surplus cross-linker. Following this, the polymer beads were dried at 60 °C for 24 h and obtained Ag@*CT*-SA/GEL polymer beads which were later used for further characterizations.

Characterizations

UV–Visible spectrophotometer (model: Shimadzu UV – 1800) was used to examine the optical characteristics of AG@*CT* NPs in the 200–800 nm wavelength range. The high-resolution transmission electron microscopy (HR-TEM) with energy-dispersive X–ray spectroscopy (EDX) image of Ag@*CT* NP was recorded using a TEM operating at an acceleration voltage of 1200 kV (Tecnai G2 F20 X-TWIN). The surface morphology of polymer beads was examined using a Field Emission Scanning Electron Microscope (Marl Zeiss, German model Zeiss Gemini SEM 300) with Energy Dispersive X-ray analysis. The structural identifications of polymer beads were analysed using the X-ray diffraction pattern obtained using the Malvern Panalytical multipurpose utilizing Cu Kα radiation with a step size of 0.02°. A scan range of 2θ = 0°—90° was used for the analysis. Bruker Alpha Platinum FT-IR spectrometer in the 4000 to 400 cm^{-1} range was used to investigate the chemical structure of *CT*, Ag@*CT* NPs, SA/GEL, and Ag@*CT*-SA/GEL beads.

Antibacterial activity

The antibacterial activities of Ag@*CT* NPs and Ag@*CT*-SA/GEL were investigated by conducting a disk diffusion method on two distinct bacterial strains [Escherichia coli (*E. coli*) (ATCC 10,536) and Staphylococcus aureus (*S. aureus*) (ATCC 25,923)] grown on nutrient agar. At specific conditions bacterial strain was inoculated onto the agar plate and then spread using an L-rod with 100 µL of dissolved Ag@*CT* NPs and Ag@*CT*-SA/GEL at varying concentrations of grown culture. Each agar plate was made by loading disks containing control (Chloramphenicol) and test compounds (Ag@*CT* NPs and Ag@*CT*-SA/GEL) which were then incubated for 24 h at 37 °C. Circular zones of inhibition surrounding the disk were determined and expressed in millimeters (mm).

Antioxidant activity

The antioxidant activities of Ag@*CT* NPs, and Ag@*CT*-SA/GEL were evaluated by 2,2-diphenyl-1-picrylhydrazyl (DPPH) assay. A solution of DPPH (0.1 µL–333 µL) in methanol was added to 1 mL of various test sample dosages in DMSO. Following a vigorous shaking, the mixture was let to remain for 30 min at ambient temperature and the absorbance at 513 nm was determined using a UV–visible spectrophotometer. L- ascorbic acid (vitamin C) was employed as the standard.

Anticancer activity

Human lung A549 cancer cell line was obtained from the American Type Culture Collection (ATCC). These cells were grown in Dulbecco's modified Eagle's medium (DMEM) supplemented with 1% Penicillin–Streptomycin and 10% Fetal Bovine Serum for cytotoxicity analysis.

The cytotoxicity of the biosynthesized Ag@*CT* NPs and *CT* extract against lung cancer cell (A549) was measured using a dimethyl thiazolyl tetrazolium bromide (MTT) assay. Each 96-well microtiter plate well received 100 µL of the diluted cell suspension, containing 50,000 cells per well and incubated for 24 h. After 24 h of incubation, a solution of Ag@*CT* NPs (test drug) at concentrations that varied from 0–100 µg/mL was applied to the generated partial monolayer. In addition, the plates were incubated in a humidified environment consisting of 95% air and 5% CO_2 for 24 h at 37 °C. Further, each well was filled with 100 µL of MTT and incubated for an additional 4 h at 37 °C with 5% CO_2. After removing the supernatant, 100 µL of DMSO was added to the plates and gently shaken to dissolve the formazan produced during the mitochondrial reduction of MTT. The absorbance was determined at 590 nm employing a microplate reader.

Apoptosis by AO/EB staining method

Acridine orange (AO) and ethidium bromide (EB) staining methods were used to validate the potential of *CT* and Ag@*CT* NPs to cause apoptosis in A549 lung cancer cells. In short, cells were placed into 24-well plates with a density of 4000 cells/well. Afterwards, the plates were kept in an incubator set at 37 °C for 24 h and then treated with the test samples. After incubating for 24 h, 10 µL of the staining solution containing 100 µg/mL of AO and 100 µg/mL of EB was introduced to each well (500 µL). Fluorescence microscope (Olympus, CKX-53, Japan) was utilized to capture the cell images immediately.

Statistical analysis

All the biological activities are performed in triplicate, and the outcomes are presented as mean ± standard deviation (SD). The statistical analysis is carried out using Graph Pad Prism program (10.1.0).

Results and discussion

Preparation of Ag@CT-SA/GEL polymer beads

Ag@*CT* NPs were mixed with SA and GEL to form a composite solution. When the mixture is dropped into a $CaCl_2$ solution, the Ca^{2+} ions instantly interact with the alginate and form a gel at the interface. On the other hand, GEL enhances mechanical characteristics and possible bioactive encapsulation. The incorporation of Ag@*CT* into SA/GEL beads can take place through chemical interactions. Electronegative carboxylate groups of SA as well as carbonyl and amine groups of GEL can form electrostatic interaction with silver metal. This interaction stabilizes the Ag NPs within the hydrogel matrix and prevents their agglomeration. Furthermore, hydroxyl groups of *CT* form hydrogen bonding interaction with SA/GEL functional groups. Figure 1 depicts the formation of Ag@*CT*-SA/GEL polymer beads.

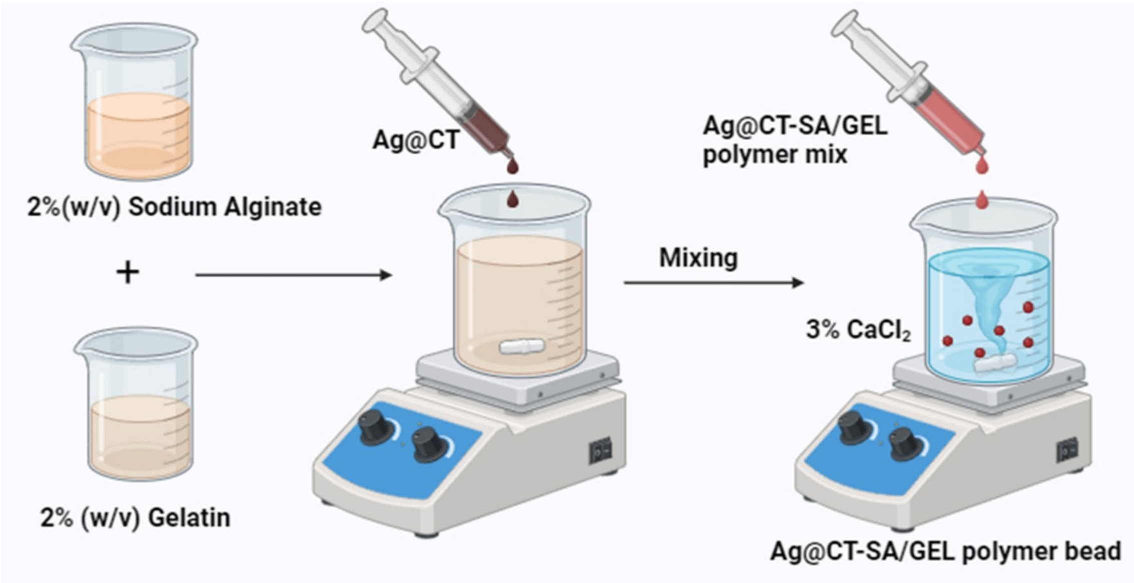

Fig. 1. Schematic representation of the formation of Ag@*CT*-SA/GEL polymer beads.

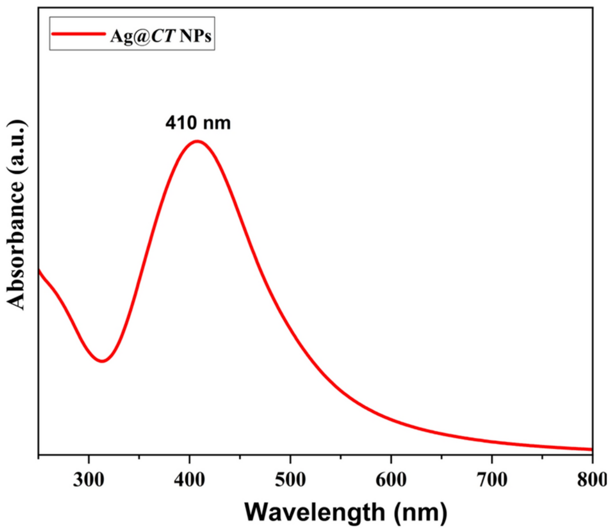

Fig. 2. UV–Visible spectrum of Ag@*CT* NPs.

UV–visible absorption spectrum

The green synthesized Ag@*CT* NPs were primarily characterized by UV–Visible spectroscopy and the absorption spectra is shown in Fig. 2. The appearance of brown color validates the reduction of Ag^{+} ions, as confirmed by the surface plasmon resonance (SPR) peak observed at 410 nm in the absorption spectra of Ag@*CT* NPs. However, our Ag@*CT* NPs demonstrate a SPR peak at lower wavelength as compared to similar *CT* based Ag NPs[40]. This lower wavelength shift is due to decrease in the particle size of Ag@*CT* NPs. Slightly modified synthetic approach may be the reason for particle size reduction in present study. The effect of size reduction is reflected in the improved antibacterial and anticancer activity of this Ag@*CT* NPs.

TEM analysis

TEM analysis was carried out to get insight into the morphology of synthesized Ag@*CT* NPs. TEM images given in Fig. 3a and b clearly illustrates uniformly distributed spherical shaped Ag NPs produced through reduction of Ag^{+} ions by *CT*. EDX analysis was performed to determine the elemental composition of Ag@*CT* NPs. The EDX spectra of Ag@*CT* NPs depicted in Fig. 3c exhibit peaks corresponding to C, O, and Ag. The existence of C and O elemental peaks in Ag@*CT* NPs account for the presence of flavonoids from *CT*.

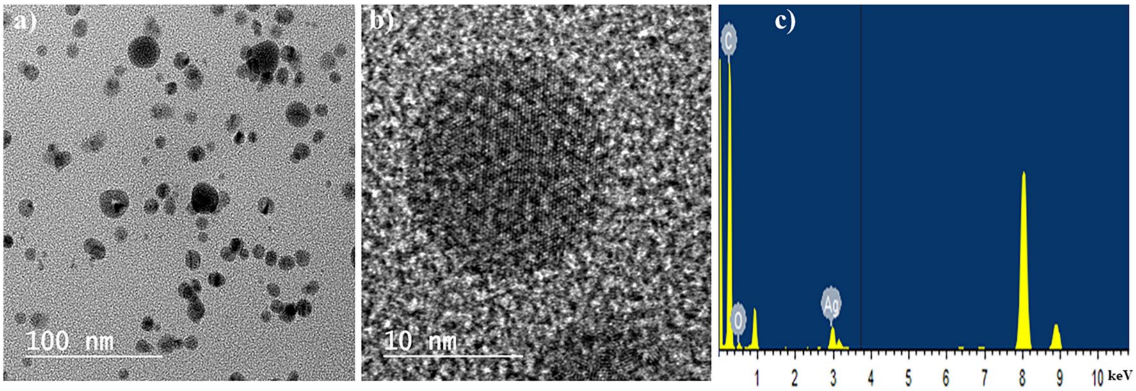

Fig. 3. HR-TEM images of Ag@*CT* NPs at various scale **(a)** 100 nm **(b)** 10 nm **(c)** EDX spectra of Ag@*CT* NPs.

SEM analysis

The surface morphologies of SA/GEL and Ag@*CT*-SA/GEL were examined by FE-SEM, as depicted in Fig. 4a and b. SEM images of SA/GEL revealed a smooth surface, whereas Ag@*CT*-SA/GEL displayed a rough surface due to the incorporation of Ag@*CT* NPs. EDX analysis of Ag@*CT*-SA/GEL is displayed in Fig. 4c. Intense carbon, oxygen peaks and less intense sodium peak in the EDX analyses reveal the presence of SA and GEL. EDX spectrum also confirms the presence of Ag@*CT* NPs in SA/GEL, as evidenced by silver peak distinct from the carbon, oxygen, and sodium peaks of SA/GEL. Additionally, elemental mapping of Ag@*CT*-SA/GEL in Fig. 4d clearly shows the homogeneous distribution of Ag@*CT* NPs in SA/GEL without any agglomeration. Figure 4e represents the elemental mapping images of C, O, Na, and Ag present in Ag@*CT*-SA/GEL.

XRD analysis

XRD analysis was used to determine the structural characteristics of the SA/GEL and, Ag@*CT*-SA/GEL as illustrated in Fig. 5. The XRD pattern of SA/GEL shows a broad peak at 2θ value 24.25° corresponding to SA due to the reflection of their (200) plane from poly-mannuronate block[41]. This broad peak also represents the amorphous nature of GEL in the sample[42]. The XRD peak of SA/GEL at 2θ value 41.46° is attributed to the reflection from the amorphous halo of SA[41]. As a result, XRD analysis confirms the presence of both SA and GEL in the polymer bead. The XRD pattern of Ag@*CT*-SA/GEL displayed 2θ peaks owing to SA/GEL as mentioned above. Along with these, it exhibits prominent diffraction peaks at 2θ values of 38.82°, 64.18° and 78.5° that represent the lattice planes of (111), (220), and (311), respectively. These peaks indicate face-centered cubic crystalline structure of metallic silver and are well align with those of ICDD file number 04–0783[43]. This verifies the presence of crystalline Ag@*CT* NPs in polymer bead[44]. This further indicates that Ag@*CT* NPs are evenly distributed throughout the polymer and retain their structural integrity. The XRD findings give substantial evidence for the successful synthesis and incorporation of Ag@*CT* NPs into the SA/GEL matrix.

FT-IR analysis

Figure 6a-d depicts the FT-IR spectra of *CT* extract, Ag@*CT* NPs, SA/GEL, and Ag@*CT*-SA/GEL. The various FT-IR peaks detected in *CT* extract enable qualitative identification of the functional groups present in it. *CT* extract shows a broad peak at 3371 cm^{-1} belongs to the stretching frequency of free hydroxyl group (–OH). The stretching vibrations of C = O and C–C bonds are responsible for the distinctive peaks located at 1631 cm^{-1} and 1386 cm^{-1}, respectively. The bending vibrational frequency of the C–O and OH present in *CT* extract is represented by the peak at 1170 cm^{-1}. A slight shift in IR peak positions of Ag@*CT* NPs in Fig. 4d, suggests the interaction of Ag with the polyphenols of *CT* extract. The absence of peak at 1170 cm^{-1} in the FT-IR spectrum of Ag@*CT* NPs suggests that the (C-O) group is responsible for capping Ag NPs[40]. The formation of SA/GEL is confirmed by the IR peaks at 3365 cm^{-1} (OH), 2335 cm^{-1} (CO_2 from atmosphere), 1643 cm^{-1} (CO–NH), 1531 cm^{-1} (C-N), 1261 cm^{-1} (C-O) and 1083 cm^{-1} (in plane C-H bending vibration)[45,46]. The characteristics peaks of SA/GEL at 1643 and 1531 cm^{-1} confirm the presence of GEL in bead[47]. Specifically, the peak at 1643 cm^{-1} reflects intermolecular interactions between alginate and gelatin[48]. The FT-IR spectrum of the Ag@*CT*-SA/GEL shows discernible alterations in all the absorption peaks when compared to the FT-IR spectrum of SA/GEL. This indicates the electrostatic interaction of Ag@*CT* with electron-rich groups of polymers[47].

Antibacterial activity

Figure 7a-d shows the possible antibacterial action of Ag@*CT* NPs and Ag@*CT*-SA/GEL against two distinct pathogenic strains such as *E. Coli* and *S. aureus* by disc diffusion method, and their results were compared with a standard antibiotic (chloramphenicol). The zone of inhibition formed is used to determine the antibacterial efficiency. The samples exhibited potent antibacterial action in a dose-dependent manner against both bacterial strains. At the concentration of 100 μg/mL, Ag@*CT* NPs demonstrated a distinct inhibitory effect against *E. coli* and *S. aureus*, producing zone of inhibition of 16 mm and 17 mm, respectively. This result is comparable to that of chloramphenicol with a zone of inhibition of 17 mm and 18 mm, respectively. These results indicate the potential antibacterial activity of Ag@*CT* NPs. The antibacterial activity of present study is substantially higher

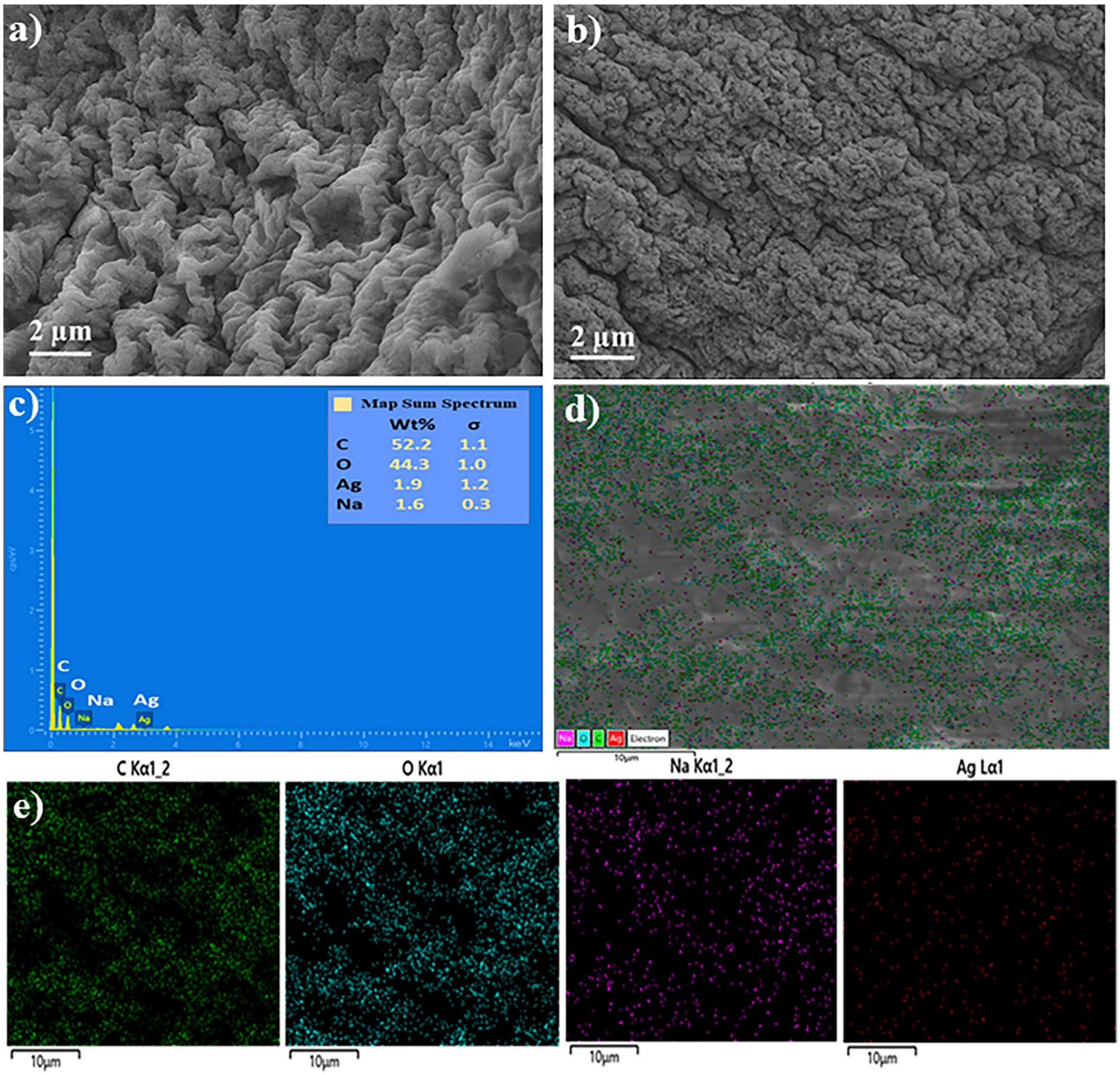

Fig. 4. SEM images of **(a)** SA/GEL and **(b)** Ag@*CT*-SA/GEL, **(c)** EDX spectra of Ag@*CT*-SA/GEL, **(d)** merged elemental distribution image of Ag@*CT*-SA/GEL **(e)** individual distribution images of elements.

than that of *CT*-based Ag NPs reported in the literature[49]. Ag@*CT*-SA/GEL at the concentration of 100 µg/mL demonstrated a zone of inhibition of 17 mm and 15 mm, respectively. Similarly, antibacterial activity of this one is comparable to that of chloramphenicol which produced a zone of inhibition of 18 mm for each bacterial strain. The polymer matrix releases Ag^+ ions from Ag@*CT*. These Ag^+ ions diffuse through cavities and surface voids of the polymer matrix and interact with bacterial cells. Moreover, hydrophilic SA has prolonged residence time that increases the local drug concentration and thereby increases the antibacterial activity of Ag@*CT*[50]. The antibacterial activity of Ag@*CT*-SA/GEL is better than that of SA/GEL based Ag NPs reported elsewhere[47].

Figure 8 depicts the mechanism by which Ag NPs exhibit antibacterial properties. Initially, Ag NPs can adhere to the bacterial cell membrane and damage its integrity. The Ag NPs can then enter the cytoplasm and exert direct or indirect interactions with a variety of macromolecules such as DNA and proteins. The oxidative stress induced by Ag NPs play a crucial role in antibacterial activity. SA/GEL polymer matrix releases Ag^+ ions from Ag@*CT*, which react with oxygen and water to generate ROS including H_2O_2, superoxide anion (O_2^-), hydroxyl radical ($OH^•$), and singlet oxygen. The produced ROS trigger lipid peroxidation in bacterial cell membrane and damage membrane integrity. This causes cellular leakage and eventual cell death. Additionally, ROS can oxidize bacterial cell proteins, causing them to lose their functional integrity. This impairs basic cellular functions like metabolism, replication, and cell division. ROS have the potential to break DNA strands and induce alterations in the base. It prevents bacteria from replicating and repairing their genomes and ultimately cause cell death. Thus, Ag NPs are highly effective to wide range of bacterial strains[51].

Antioxidant activity

CT extract known for its potent antioxidant activity due to the presence of various polyphenols. We wanted to check whether synthesized Ag@*CT* NPs and Ag@*CT*-SA/GEL still possess antioxidant properties or not.

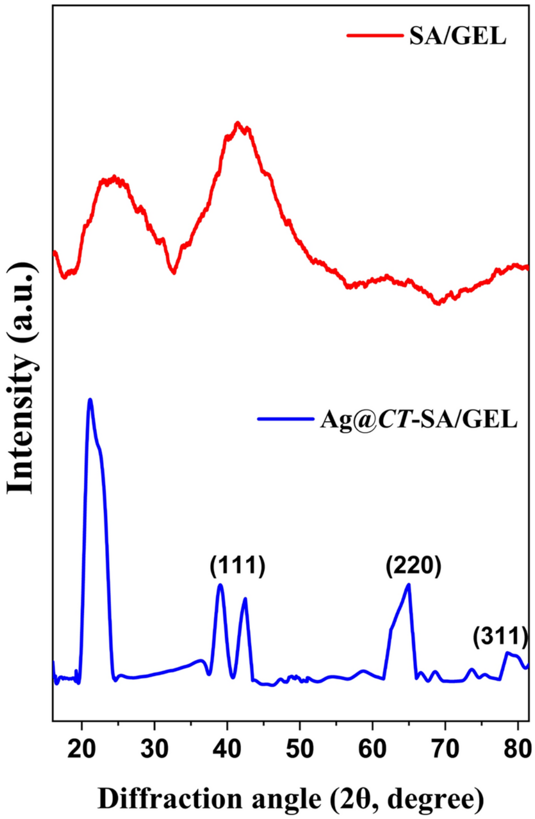

Fig. 5. XRD pattern of SA/GEL and Ag@*CT*-SA/GEL.

Antioxidant property is required to maintain low to moderate ROS concentration which is important for the normal physiological functioning of cell. Therefore, the antioxidant activities of Ag@*CT* NPs, and Ag@*CT*-SA/GEL were determined by performing DPPH assay as shown in Fig. 9. The graph illustrates that the radical scavenging activities of Ag@*CT* NPs, and Ag@*CT*-SA/GEL were rose steadily by increasing the concentration corresponding with ascorbic acid (control). At 50 µg/mL, Ag@*CT* NPs demonstrated 64.2% ± 0.0049 radical scavenging activity, while Ag@*CT*-SA/GEL exhibited considerably higher activity of 68% ± 0.0051. On the other hand, the control ascorbic acid possesses radical scavenging activity of 82.32% ± 0.0657. The results suggest that Ag@*CT*-SA/GEL has antioxidant activity which making it suitable for anticancer applications. Ag@*CT* NPs and Ag@*CT*-SA/GEL exhibited better DPPH radical scavenging activities as compared to that of previously reported literature study[52,53].

Anticancer activity

The anticancer potential of Ag@*CT* NPs and *CT* was assessed using the MTT test on A549 human lung cancer cell line at various doses (0–100 µg/mL). The percentage of cell viability in relation to different *CT* and Ag@*CT* NPs concentrations is shown in the Fig. 10. The cell viability percentage of *CT* at 10 µg/mL was 92% ± 0.0036 that decreased to 50% ± 0.0011 at 50 µg/mL. Then, viability was reduced to 3% ± 0.0126 as the concentration reached 100 µg/mL. Similarly, Ag@*CT* NPs displayed cell viability percentage of 93% ± 0.0057 at 10 µg/mL and it reduced to 52% ± 0.0225 at 50 µg/mL. As the concentration reaches 100 µg/mL, viability of Ag@*CT* NPs was further reduced to 6% ± 0.0031. The IC_{50} values for the plant extract and Ag@*CT* NPs against the A549 cells were determined to be 50.92 ± 0.05 µg/mL and 51.35 ± 0.05 µg/mL, respectively. Table 1 summarizes a comparative investigation of the anticancer effects of literature reported Ag NPs and present study against lung cancer cell. It is clear from the table that Ag@*CT* NPs demonstrated enhanced cytotoxicity.

Figure 11a-d demonstrate the phase contrast microscopy images of A549 cell line before and after treatment with *CT* and Ag@*CT* NPs. The image clearly shows that *CT* and Ag@*CT* NPs treated cells showed morphological changes, such as cell clustering, loss of membrane integrity, chromatin condensation, and inhibition of cell growth in A549 cells. These results demonstrate that at the investigated concentrations, *CT* and Ag@*CT* NPs treated A549 cells experience cell death while untreated cells maintain viability. Hence, obtained results support the anticancer action of biogenic Ag@*CT* NPs.

Figure 12 depicts the anticancer mechanism of Ag@*CT* NPs. It has been proposed that there are a few possible mechanisms via which Ag NPs and cancer cells interact, including endocytosis-mediated internalization of the NPs, electrostatic interaction between the Ag NPs and the cell surface, and NPs grabbed by cell receptors[61,62]. Ag NPs can generate ROS within the cell, which can cause damage to DNA, disruption of the mitochondria, oxidation of proteins, and ultimately, that may lead to cell death[10]. Furthermore, Ag NPs are better candidate

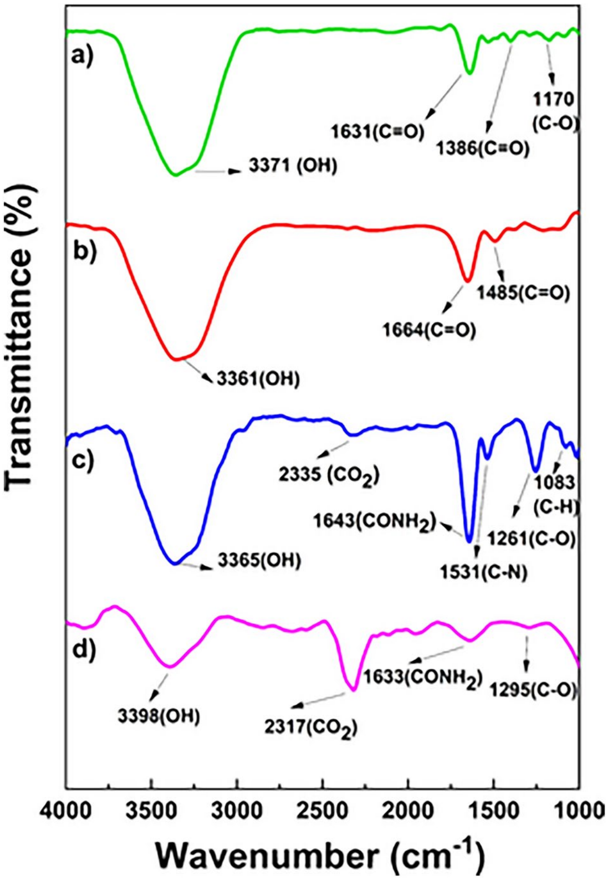

Fig. 6. FT-IR spectrum of **(a)** *CT* **(b)** Ag@*CT* NPs **(c)** SA/GEL and **(d)** Ag@*CT*-SA/GEL.

for anticancer activity because of their capacity to control pH-dependent release, induce hyperthermia inside cancer cells[63,64].

Apoptosis by AO/EB staining method

The apoptotic potential of *CT* and Ag@*CT* NPs was validated using AO/EB staining of A549 cells. The cells were treated with respective IC_{50} concentrations of test samples for 24 h and the apoptotic changes were observed using fluorescence microscopy along with AO/EB staining. AO enters the cell membrane, and normal cells emit green fluorescence. When cells lose the integrity of their cytoplasmic membrane, they engage EB, an intercalating agent, which causes the nuclei to appear red under fluorescence microscopy. Early apoptotic cells have condensed/fragmented chromatin with a bright green nucleus, whereas the viable cells have diffused chromatin appear in green nucleus. Apoptotic cells, or apoptotic bodies, develop as a result of nuclear shrinkage and blebbing, which is visible as orange-colored nucleus. On the other hand, necrotic cells exhibited red fluorescence, indicating membrane damage. As seen in Fig. 13a and c, control cells showed no morphological alterations and displayed homogeneous green fluorescence in both the cytoplasm and nuclei. A549 cells treated with *CT* and Ag@*CT* NPs exhibited red fluorescence as given in Fig. 13b and d. The observed morphological alterations and increased red fluorescence indicate that Ag@*CT* NP is more effective than *CT* in killing A549 lung cancer cells via apoptosis. The results confirm that Ag@*CT* NPs caused cell death by apoptosis, resulting in chromatin condensation and nuclear disintegration.

Conclusion

Ag@*CT*-SA/GEL was prepared by physical crosslinking with $CaCl_2$. The effective incorporation of Ag@*CT* NPs into the SA/GEL has been confirmed by various spectroscopic analysis. The Ag@*CT*-SA/GEL demonstrated remarkable antibacterial capabilities against both gram-positive and gram-negative bacterial strains, confirming the polymer bead's ability to release Ag@*CT* NPs at the infection site. The Ag@*CT* NPs and Ag@*CT*-SA/GEL displayed a promising DPPH scavenging activity. Moreover, the MTT assay revealed that Ag@*CT* NPs exhibited cytotoxicity against A549 cancer cells with an IC_{50} value of 51.35 ± 0.05 μg/mL. The apoptosis of A549 cells caused by Ag@*CT* NPs was also confirmed by AO/EB staining method. Therefore, the Ag@*CT*-SA/GEL polymer beads can be the promising candidate for antibacterial and anticancer applications.

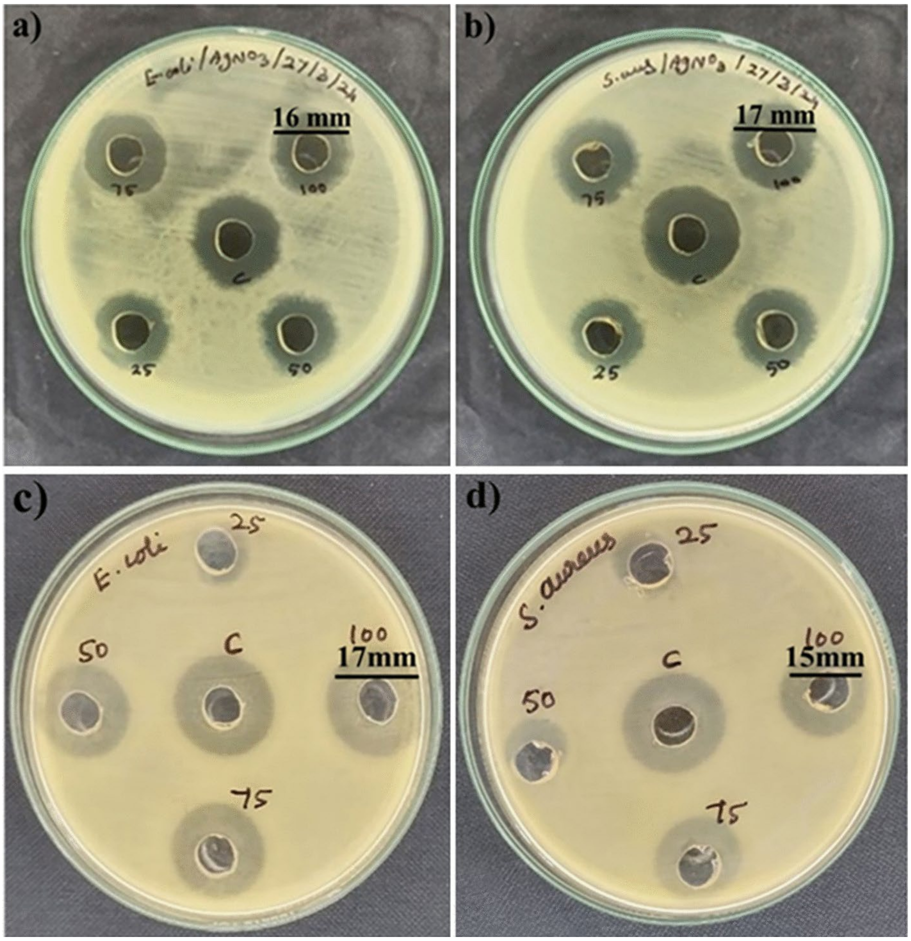

Fig. 7. Antibacterial activity of Ag@*CT* NPs tested against **(a)***E. coli*(**b**)*S. aureus* & antibacterial activity of Ag@*CT*-SA/GEL polymer bead tested against (**c**)*E. coli*(**d**)*S. aureus*.

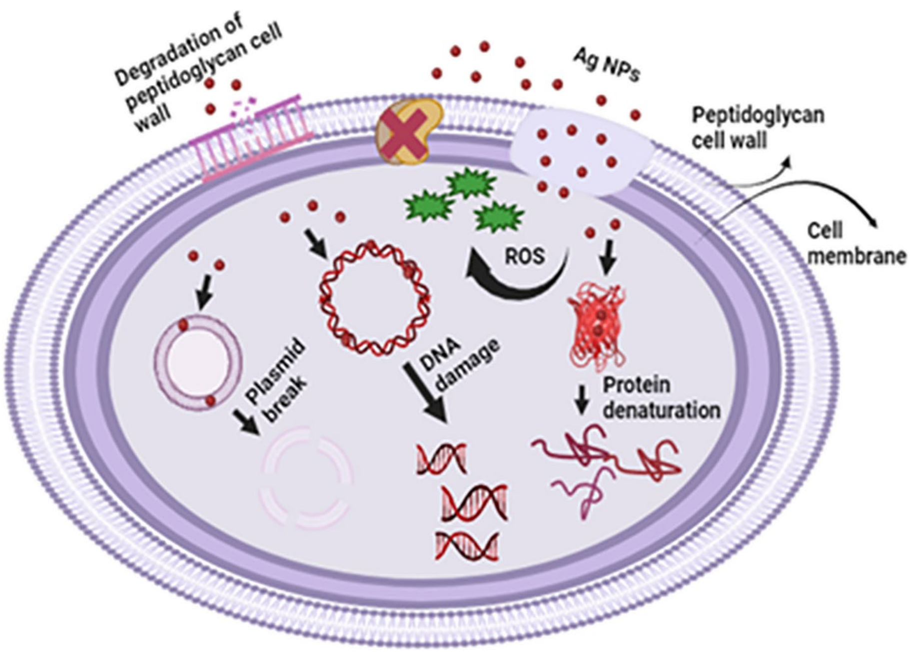

Fig. 8. Antibacterial mechanism of Ag NPs.

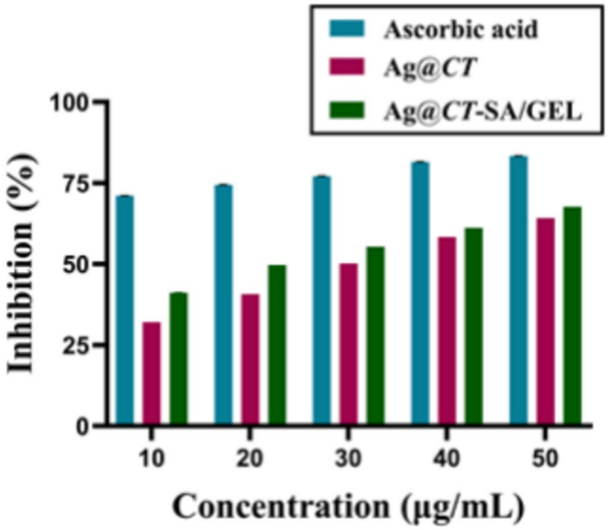

Fig. 9. Antioxidant activity of Ag@*CT* NPs, Ag@*CT*-SA/GEL and control. Data is expressed as mean ± SD (n = 3).

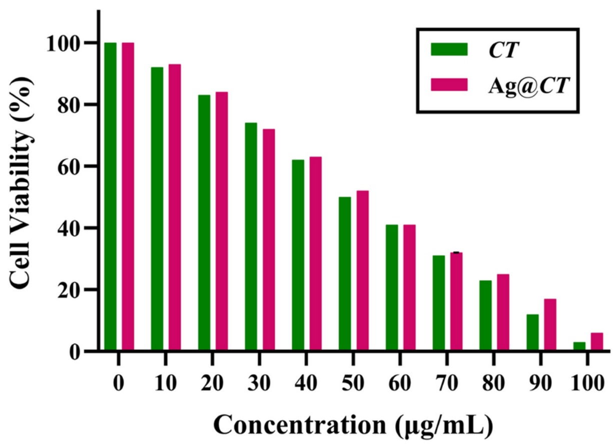

Fig. 10. % Cell viability of *CT* and Ag-@*CT* NPs against A549 cells. The data is expressed as mean ± SD (n = 3).

S.No	NPs	IC_{50}	References
1	Ag NPs	62.82 μg/mL	[54]
2	Ag NPs	75 μg/mL	[55]
3	Ag NPs	60 μg/mL	[56]
4	Ag NPs	328 μg/mL	[57]
5	Ag NPs	100 μg/mL	[58]
6	Ag NPs	118.50 ± 0.29 μg/mL	[59]
7	Ag NPs	65.17 μg/mL	[60]
8	Ag@*CT* NPs	51.35 ± 0.05 μg/mL	Present study

Table 1. Comparative study of IC_{50} values of different biogenic Ag NPs.

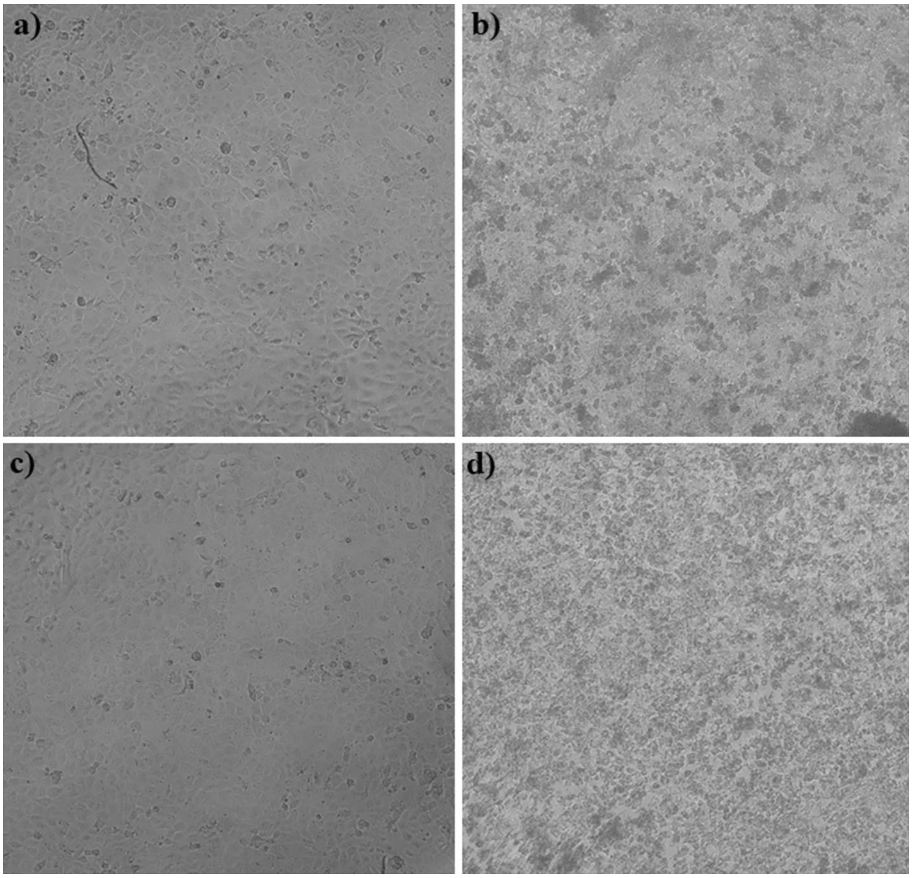

Fig. 11. Morphological appearance of A549 cells in phase contrast microscopy for **(a)** Control **(b)***CT* and **(c)** Control **(d)** Ag@*CT* NPs.

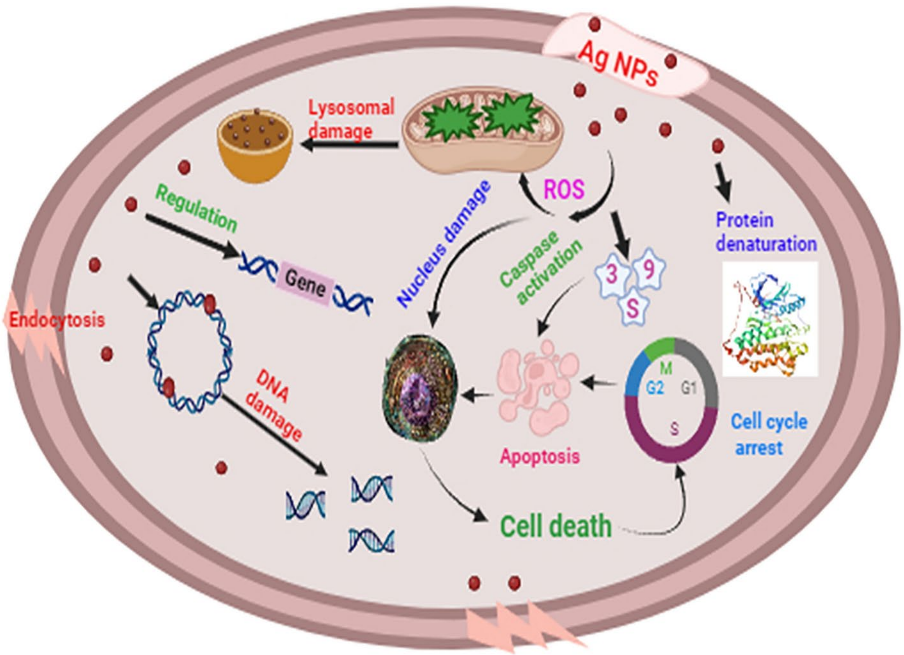

Fig. 12. Anticancer mechanism of Ag NPs.

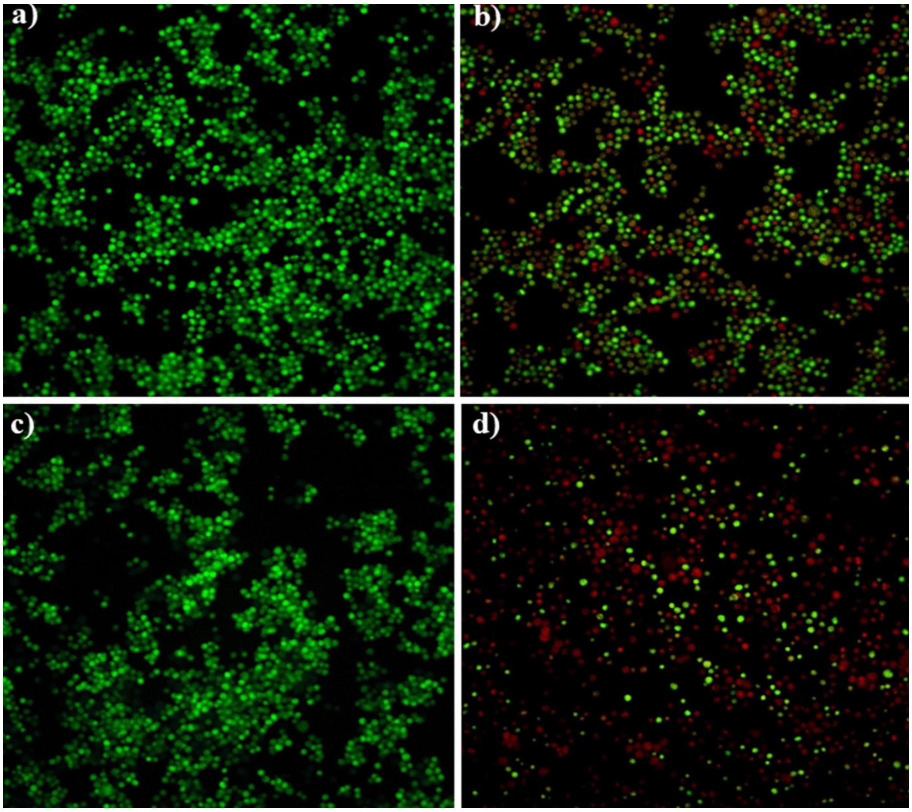

Fig. 13. Apoptotic development and morphological changes in A549 lung cancer cells upon treatment with **(a)** control **(b)***CT***(c)** control and **(d)** Ag@*CT* NPs.

Data availability

The datasets used and/or analysed during the current study available from the corresponding author on reasonable request.

Received: 30 August 2024; Accepted: 5 November 2024
Published online: 08 November 2024

References

1. Bray, F. et al. Global cancer statistics 2018: GLOBOCAN estimates of incidence and mortality worldwide for 36 cancers in 185 countries. *CA. Cancer J. Clin.* **68**, 394–424 (2018).
2. Das, C. G. A. et al. Antibacterial activity of silver nanoparticles (biosynthesis): A short review on recent advances. *Biocatal. Agric. Biotechnol.* **27**, 101593 (2020).
3. Kaushal, A. et al. Advances in therapeutic applications of silver nanoparticles. *Chem. Biol. Interact.* **382**, 110590 (2023).
4. Sandra, S. et al. Synthesis of electrospun PVA/chitosan nanofibrous scaffold impregnated with CuO nanoparticles for wound healing. *Cellulose* **31**, 6387–6401 (2024).
5. Niveditha, S. et al. Wound healing applications of β-cyclodextrin capped zinc sulphide nanoparticles impregnated electrospun polymeric nanofibrous scaffold. *J. Drug Deliv. Sci. Technol.* **95**, 105597 (2024).
6. Santhosh, A., Theertha, V., Prakash, P. & Smitha Chandran, S. From waste to a value added product: Green synthesis of silver nanoparticles from onion peels together with its diverse applications. *Mater. Today Proc.* **46**, 4460–4463 (2019).
7. Lansdown, A. B. G. A pharmacological and toxicological profile of silver as an antimicrobial agent in medical devices. *Adv. Pharmacol. Sci.* (2010).
8. Arora, S., Jain, J., Rajwade, J. M. & Paknikar, K. M. Cellular responses induced by silver nanoparticles: *In vitro* studies. *Toxicol. Lett.* **179**, 93–100 (2008).
9. Ahmadian, E. et al. Effect of silver nanoparticles in the induction of apoptosis on human hepatocellular carcinoma (HepG2) cell line. *Mater. Sci. Eng. C* **93**, 465–471 (2018).
10. Eom, H. J. & Choi, J. p38 MAPK activation, DNA damage, cell cycle arrest and apoptosis as mechanisms of toxicity of silver nanoparticles in Jurkat T cells. *Environ. Sci. Technol.* **44**, 8337–8342 (2010).
11. Zahoor, I. et al. Viburnum nervosum Leaf Extract Mediated Green Synthesis of Silver Nanoparticles: A Viable Approach to Increase the Efficacy of an Anticancer Drug. *Anticancer. Agents Med. Chem.* **21**, 1266–1274 (2020).
12. Pugazhenthi, E. *et al.* "Cleome rutidosperma leaf extract mediated biosynthesis of silver nanoparticles and anti-candidal, anti-biofilm, anti-cancer, and molecular docking analysis". *Biomass Convers. Biorefinery* 1–13 (2023).
13. Abaid, R. et al. Biosynthesizing Cassia fistula Extract-Mediated Silver Nanoparticles for MCF-7 Cell Lines Anti-Cancer Assay. *ACS Omega* **8**, 17317–17326 (2023).
14. Patil, A. P. & Patil, V. R. Clitoria ternatea Linn.: an overview. *Int J Pharm Res.* **3**, 20–23 (2011).
15. Mukherjee, P. K., Kumar, V., Kumar, N. S. & Heinrich, M. The Ayurvedic medicine Clitoria ternatea-From traditional use to scientific assessment. *J. Ethnopharmacol.* **120**, 291–301 (2008).
16. Dave, A., Parande, F., Park, E. J. & Pezzuto, J. M. Phytochemicals and cancer chemoprevention. *J. Cancer Metastasis Treat.* **6**, (2020).

17. Ravishankar, D., Rajora, A. K., Greco, F. & Osborn, H. M. I. Flavonoids as prospective compounds for anti-cancer therapy. *Int. J. Biochem. Cell Biol.* **45**, 2821–2831 (2013).
18. Jacob, L. & Latha, M. S. Anticancer activity of Clitoria ternatea linn. Against dalton's lymphoma. *Int. J. Pharmacogn. Phytochem. Res.* **4**, 107–112 (2013).
19. Iamsaard, S. et al. Antioxidant activity and protective effect of Clitoria ternatea flower extract on testicular damage induced by ketoconazole in rats. *J. Zhejiang Univ. Sci. B* **15**, 548–555 (2014).
20. Shen, Y. et al. Butterfly pea (Clitoria ternatea) seed and petal extracts decreased HEp-2 carcinoma cell viability. *Int. J. Food Sci. Technol.* **51**, 1860–1868 (2016).
21. Rahman, A. S. et al. Bioactivity guided cytotoxic activity of Clitoria ternatea utilizing brine shrimp lethality bioassay. *Bangladesh J Physiol Pharmacol* https://doi.org/10.3329/bjpp.v22i1.3564 (1970).
22. Krithiga, N., Rajalakshmi, A. & Jayachitra, A. Green Synthesis of Silver Nanoparticles Using Leaf Extracts of Clitoria ternatea and Solanum nigrum and Study of Its Antibacterial Effect against Common Nosocomial Pathogens. *J. Nanosci.* https://doi.org/10.1155/2015/928204 (2015).
23. Malabadi, R. B., Mulgund, G. S., Meti, N. T., Nataraja, K. & Vijaya Kumar, S. Antibacterial activity of silver nanoparticles synthesized by using whole plant extracts of Clitoria ternatea. *Res Pharm* **2**, 10–21 (2012).
24. Manokari, M. & Shekhawat, M. S. Synthesis of Zinc oxide nanoparticles from Clitoria ternatea L. extracts: a green approach. *World Sci. News.* **52**, 216–227 (2016).
25. Fatimah, I., Hidayat, H., Nugroho, B. H. & Husein, S. Ultrasound-assisted biosynthesis of silver and gold nanoparticles using Clitoria ternatea flower. *South African J. Chem. Eng.* **34**, 97–106 (2020).
26. Srinivas, B. K., Shivamadhu, M. C., Siddappaji, K. K., Krishnappa, D. K. & Jayarama, S. Angiosuppressive effects of bio-fabricated silver nanoparticles synthesis using Clitoria ternatea flower: an *in vitro* and in vivo approach. *J. Biol. Inorg. Chem.* **24**, 1115–1126 (2019).
27. Pérez-Vicente, A., Gil-Izquierdo, A. & García-Viguera, C. *In vitro* gastrointestinal digestion study of pomegranate juice phenolic compounds, anthocyanins, and vitamin C. *J. Agric. Food Chem.* **50**, 2308–2312 (2002).
28. Munin, A. & Edwards-Lévy, F. Encapsulation of natural polyphenolic compounds; a review. *Pharmaceutics.* **3**, 793–829 (2011).
29. Ye, S. *et al.* Alginates from Brown Seaweeds as a Promising Natural Source: A Review of Its Properties and Health Benefits. *Food Rev. Int.* 1–29 (2023).
30. Sudarsan, S. et al. Ecofriendly pH-Tunable Hydrogels for Removal of Perilous Thiazine Dye. *J. Polym. Environ.* **26**, 3773–3784 (2018).
31. Sudarsan, S., Franklin, D. S., Sakthivel, M. & Guhanathan, S. Non toxic, antibacterial, biodegradable hydrogels with pH-stimuli sensitivity: Investigation of swelling parameters. *Carbohydr. Polym.* **148**, 206–215 (2016).
32. Li, Q. et al. Fabrication and characterization of Ca(II)-alginate-based beads combined with different polysaccharides as vehicles for delivery, release and storage of tea polyphenols. *Food Hydrocoll.* https://doi.org/10.1016/j.foodhyd.2020.106274 (2021).
33. John, M. et al. Injectable Tissue Adhesive Microgel Composite Containing Antifibrotic Drug for Vocal Fold Scarring. *ACS Appl. Bio Mater.* **7**, 5237–5246 (2024).
34. Tondera, C. et al. Gelatin-based hydrogel degradation and tissue interaction in vivo: Insights from multimodal preclinical imaging in immunocompetent nude mice. *Theranostics* **6**, 2114–2128 (2016).
35. Hu, C., Lu, W., Mata, A., Nishinari, K. & Fang, Y. Ions-induced gelation of alginate: Mechanisms and applications. *Int. J. Biol. Macromol.* **177**, 578–588 (2021).
36. Sanchez-Ballester, N. M., Soulairol, I., Bataille, B. & Sharkawi, T. Flexible heteroionic calcium-magnesium alginate beads for controlled drug release. *Carbohydr. Polym.* **207**, 224–229 (2019).
37. Liu, N. N. et al. The intratumor mycobiome promotes lung cancer progression via myeloid-derived suppressor cells. *Cancer Cell* **41**, 1927–1944 (2023).
38. Rahal, Z. & Kadara, H. Beyond bacteria: How the intratumor mycobiome modulates lung adenocarcinoma progression. *Cancer Cell* **41**, 1846–1848 (2023).
39. Shree Haripriya, B., Anakha, D. R., Yamuna, R., Vinoba, M. & Bhagiyalakshmi, M. Green synthesized AgNPs using Clitoria ternatea extract and its confinement on SBA-15/GPTMS-TAEA for controlled drug release of ciprofloxacin. *J. Porous Mater.* **31**, 351–363 (2024).
40. Khwannimit, D., Maungchang, R. & Rattanakit, P. Green synthesis of silver nanoparticles using Clitoria ternatea flower: an efficient catalyst for removal of methyl orange. *Int. J. Environ. Anal. Chem.* **17**, 5247–5263 (2020).
41. Feyissa, Z., Edossa, G. D., Gupta, N. K. & Negera, D. Development of double crosslinked sodium alginate/chitosan based hydrogels for controlled release of metronidazole and its antibacterial activity. *Heliyon* **9**, 20144 (2023).
42. Kamal, T. et al. Silver Nanoparticles Embedded in Gelatin Biopolymer Hydrogel as Catalyst for Reductive Degradation of Pollutants. *J. Polym. Environ.* **28**, 399–410 (2020).
43. Abou-Zeid, R. E., Awwad, N. S., Nabil, S., Salama, A. & Youssef, M. A. Oxidized alginate/gelatin decorated silver nanoparticles as new nanocomposite for dye adsorption. *Int. J. Biol. Macromol.* **141**, 1280–1286 (2019).
44. Sethi, S. et al. Biopolymer starch-gelatin embedded with silver nanoparticle–based hydrogel composites for antibacterial application. *Biomass Convers. Biorefinery* **12**, 5363–5384 (2022).
45. Lopes, S., Bueno, L., De Aguiar Júnior, F. & Finkler, C. L. L. Preparation and characterization of alginate and gelatin microcapsules containing Lactobacillus Rhamnosus. *An. Acad. Bras. Cienc.* **89**, 1601–1613 (2017).
46. Eivazzadeh-Keihan, R. et al. Fabrication of a magnetic alginate-silk fibroin hydrogel, containing halloysite nanotubes as a novel nanocomposite for biological and hyperthermia applications. *Sci. Rep.* **12**, 1–13 (2022).
47. Li, H. et al. Preparation and characterization of sodium alginate/gelatin/Ag nanocomposite antibacterial film and its application in the preservation of tangerine. *Food Packag. Shelf Life* **33**, 100928 (2022).
48. Abbasiliasi, S. et al. Use of sodium alginate in the preparation of gelatin-based hard capsule shells and their evaluation: *In vitro*. *RSC Adv.* **9**, 16147–16157 (2019).
49. Citradewi, P. W., Hidayat, H., Purwiandono, G., Fatimah, I. & Sagadevan, S. Clitorea ternatea-mediated silver nanoparticle-doped hydroxyapatite derived from cockle shell as antibacterial material. *Chem. Phys. Lett.* **769**, 138412 (2021).
50. Sudarsan, S. et al. Nontoxic pH-sensitive silver nanocomposite hydrogels for potential wound healing applications. *Polym. Technol. Mater.* **60**, 84–104 (2020).
51. Dakal, T. C., Kumar, A., Majumdar, R. S. & Yadav, V. Mechanistic basis of antimicrobial actions of silver nanoparticles. *Front. Microbiol.* **7**, 1–17 (2016).
52. Feng, Q., Fan, B. & He, Y. C. Antibacterial, antioxidant, Cr(VI) adsorption and dye adsorption effects of biochar-based silver nanoparticles-sodium alginate-tannic acid composite gel beads. *Int. J. Biol. Macromol.* **271**, 132453 (2024).
53. Arghand, N., Reiisi, S., Karimi, B., Khorasgani, E. M. & Heidari, R. Biosynthesis of Nanocomposite Alginate-Chitosan Loaded with Silver Nanoparticles Coated with Eugenol/Quercetin to Enhance Wound Healing. *Bionanoscience* https://doi.org/10.1007/s12668-024-01479-w (2024).
54. Dadashpour, M. et al. Biomimetic synthesis of silver nanoparticles using Matricaria chamomilla extract and their potential anticancer activity against human lung cancer cells. *Mater. Sci. Eng. C* **92**, 902–912 (2018).
55. Rajivgandhi, G. N. et al. Synthesis of silver nanoparticle (Ag NPs) using phytochemical rich medicinal plant Lonicera japonica for improve the cytotoxicity effect in cancer cells. *J. King Saud Univ. - Sci.* **34**, 101798 (2022).

56. Lava, M. B., Muddapur, U. M., Basavegowda, N., More, S. S. & More, V. S. Characterization, anticancer, antibacterial, anti-diabetic and anti-inflammatory activities of green synthesized silver nanoparticles using Justica wynaadensis leaves extract. *Mater. Today Proc.* **46**, 5942–5947 (2020).
57. Zhang, H., Li, T., Luo, W., Peng, G. X. & Xiong, J. Green synthesis of Ag nanoparticles from Leucus aspera and its application in anticancer activity against alveolar cancer. *J. Exp. Nanosci.* **17**, 47–60 (2022).
58. Mittal, J. et al. Unveiling the cytotoxicity of phytosynthesised silver nanoparticles using Tinospora cordifolia leaves against human lung adenocarcinoma A549 cell line. *IET Nanobiotechnology* **14**, 230–238 (2020).
59. Applications to Anticancer. Vinay, S. P., Udayabhanu, Nagaraju, G., Chandrappa, C. P. & Chandrasekhar, N. Rauvolfia tetraphylla (Devil Pepper)-Mediated Green Synthesis of Ag Nanoparticles. *Antioxidant and Antimitotic. J. Clust. Sci.* **30**, 1545–1564 (2019).
60. Nayaka, S. et al. Synthesis of biogenic silver nanoparticles using zanthoxylum rhetsa (Roxb) dc seed coat extract as reducing agent and in-vitro assessment of anticancer effect on a549 lung cancer cell line. *Int. J. Pharm. Res.* **12**, 302–314 (2020).
61. Valdiglesias, V. Cytotoxicity and Genotoxicity of Nanomaterials. *Nanomaterials* **12**, 279–290 (2022).
62. AshaRani, P. V., Hande, M. P. & Valiyaveettil, S. Anti-proliferative activity of silver nanoparticles. *BMC Cell Biol.* **10**, 65 (2009).
63. Nezami, S. & Sadeghi, M. pH-sensitive free AgNPs composite and nanocomposite beads based on starch as drug delivery systems. *Polym. Bull.* **77**, 1255–1279 (2020).
64. Munir, T. et al. Treatment of breast cancer with capped magnetic-NPs induced hyperthermia therapy. *J. Mol. Struct.* **1196**, 88–95 (2019).

Acknowledgements
We are thankful to COE-AMGT (MHRD, New Delhi) center for the instrumental facilities.

Author contributions
V.T.V. and V.J. wrote the main manuscript, Methodology, Formal analysis and Data analysis. V.A. did Methodology and Data collection. A.D.R. and S.K. did Data collection. R.Y. did Design of experiments, Visualization, supervision, conceptualization, validation, reviewing and editing. All authors reviewed the manuscript.

Declarations

Competing interests
The authors declare no competing interests.

Ethical approval
No humans or animals' subjects used for this study.

Additional information
Correspondence and requests for materials should be addressed to R.Y.